NASA/TM-20230008104

Benefits of Ka-band GaN MMIC High Power Amplifiers With Wide Bandwidth and High Spectral/Power Added Efficiencies for Cognitive Radio Platforms

Rainee N. Simons, Adam M. Gannon, Joseph A. Downey, Marie T. Piasecki, and Bryan L. Schoenholz
Glenn Research Center, Cleveland, Ohio

July 2023

NASA STI Program . . . in Profile

Since its founding, NASA has been dedicated to the advancement of aeronautics and space science. The NASA Scientific and Technical Information (STI) Program plays a key part in helping NASA maintain this important role.

The NASA STI Program operates under the auspices of the Agency Chief Information Officer. It collects, organizes, provides for archiving, and disseminates NASA's STI. The NASA STI Program provides access to the NASA Technical Report Server—Registered (NTRS Reg) and NASA Technical Report Server—Public (NTRS) thus providing one of the largest collections of aeronautical and space science STI in the world. Results are published in both non-NASA channels and by NASA in the NASA STI Report Series, which includes the following report types:

- TECHNICAL PUBLICATION. Reports of completed research or a major significant phase of research that present the results of NASA programs and include extensive data or theoretical analysis. Includes compilations of significant scientific and technical data and information deemed to be of continuing reference value. NASA counter-part of peer-reviewed formal professional papers, but has less stringent limitations on manuscript length and extent of graphic presentations.

- TECHNICAL MEMORANDUM. Scientific and technical findings that are preliminary or of specialized interest, e.g., "quick-release" reports, working papers, and bibliographies that contain minimal annotation. Does not contain extensive analysis.

- CONTRACTOR REPORT. Scientific and technical findings by NASA-sponsored contractors and grantees.

- CONFERENCE PUBLICATION. Collected papers from scientific and technical conferences, symposia, seminars, or other meetings sponsored or co-sponsored by NASA.

- SPECIAL PUBLICATION. Scientific, technical, or historical information from NASA programs, projects, and missions, often concerned with subjects having substantial public interest.

- TECHNICAL TRANSLATION. English-language translations of foreign scientific and technical material pertinent to NASA's mission.

For more information about the NASA STI program, see the following:

- Access the NASA STI program home page at http://www.sti.nasa.gov

- E-mail your question to help@sti.nasa.gov

- Fax your question to the NASA STI Information Desk at 757-864-6500

- Telephone the NASA STI Information Desk at 757-864-9658

- Write to:
  NASA STI Program
  Mail Stop 148
  NASA Langley Research Center
  Hampton, VA 23681-2199

NASA/TM-20230008104

Benefits of Ka-band GaN MMIC High Power Amplifiers With Wide Bandwidth and High Spectral/Power Added Efficiencies for Cognitive Radio Platforms

Rainee N. Simons, Adam M. Gannon, Joseph A. Downey, Marie T. Piasecki, and Bryan L. Schoenholz
Glenn Research Center, Cleveland, Ohio

National Aeronautics and
Space Administration

Glenn Research Center
Cleveland, Ohio 44135

July 2023

Acknowledgments

The authors would like to thank Nicholas Varaljay for installing the DC bias harness on the HPAs and the Space Communications and Navigation (SCaN) Program for their support. This NASA Technical Memorandum (TM) is an expanded version of the paper presented at the virtual 4th NASA and IEEE Cognitive Communications for Aerospace Applications (CCAA) Workshop 2023, June 20 to 22, 2023. The Figures for this NASA TM are archived under E-20127.

The authors would like to thank Rohde & Schwarz for the trial license for R&S FSW-K17 Multi-Carrier Group Delay measurement software.

This report contains preliminary findings, subject to revision as analysis proceeds.

Level of Review: This material has been technically reviewed by technical management.

This report is available in electronic form at https://www.sti.nasa.gov/ and https://ntrs.nasa.gov/

Benefits of Ka-band GaN MMIC High Power Amplifiers With Wide Bandwidth and High Spectral/Power Added Efficiencies for Cognitive Radio Platforms

Rainee N. Simons, Adam M. Gannon, Joseph A. Downey, Marie T. Piasecki, and Bryan L. Schoenholz
National Aeronautics and Space Administration
Glenn Research Center
Cleveland, Ohio 44135

Abstract

A cognitive radio on a future NASA near-Earth spacecraft will be capable of sensing its environment and dynamically adapting its operating parameters to provide the desired SATCOM service to the mission. A key component that can enable this type of operation is a high-power amplifier (HPA) that resides on the radio platform. In this report, we present the RF performance characteristics of a Ka-band gallium nitride (GaN) monolithic microwave integrated circuit (MMIC) based HPA for cognitive radio platforms. These characteristics include the output power, gain, power added efficiency (PAE), RMS error vector magnitude (EVM), spectral efficiency, 3rd-order intermodulation distortion (IMD) products, spectrum, spectral regrowth, noise figure (NF), phase noise, and group delay. The data presented indicates that the HPA meets NTIA, military, and commercial spectral mask requirements. In addition, we discuss the benefits offered by the above performance characteristics toward the design and implementation of a cognitive radio platform. Furthermore, as examples, we discuss three potential use cases that apply artificial intelligence (AI) and machine learning (ML) techniques and exploit the performance characteristics discussed above to provide a knowledge-based cognitive radio platform design for SATCOM. Thus, cognitive radios with performance flexibility can enable roaming and provide seamless interoperability autonomously in the future between NASA, commercial, and other space networks owned by U.S. government agencies.

1.0 Introduction

As of now, a significant portion of the space communications, navigation, timing, and tracking infrastructure in the U.S. is owned and operated by NASA. NASA plans to transition the above infrastructure in a phased manner to commercial SATCOM networks in the next decade (Ref. 1). One of the challenges to be overcome is developing new radios for user spacecraft terminals that are capable of roaming and have performance flexibility to interoperate across multiple commercial service provider networks and space networks owned by U.S. government agencies (Refs. 2 and 3). On the other hand, advances in artificial intelligence (AI) and machine learning (ML) are taking place and have enabled the microwave community to create breakthrough capabilities in semiconductor devices, integrated circuits, and systems as described in a recent special issue on this topic (Ref. 4). Additionally, research in artificial neural networks (ANNs) has demonstrated new training algorithms that enable satellite systems to learn from the environment surrounding them and adaptively allocate onboard resources to enhance performance and spectrum efficiency (Refs. 5 to 7).

Consequently, the developers of new radios for user spacecraft are investigating the application of AI, ML, and ANN based advanced software training algorithms to optimize link performance in the presence of changing communications conditions. These cognitive radios can learn from the environment in which they are operating, then adaptively and dynamically change the operating frequency, effective isotropic radiated power (EIRP), bandwidth, waveforms, data rates, and protocols as outlined in SCaN's vision for the future (Ref. 8). An integral part of the cognitive radio is a microwave wideband high-power amplifier (HPA) that facilitates the above changes. In the past, several researchers have investigated power amplifiers (PAs) for cognitive radio applications. In Reference 9, a 3.0 to 7.5 GHz PA is demonstrated in 0.15-μm indium gallium arsenide (InGaAs) pseudomorphic high electron mobility transistor (HEMT) technology; in Reference 10, a 450 to 730 MHz PA is demonstrated in 0.18-μm complementary metal oxide semiconductor (CMOS) process; in Reference 11, a 1.0 to 5.0 GHz PA is demonstrated in 0.18-μm CMOS process.

This report builds on our prior and ongoing efforts in cognitive radios (Ref. 12), cognitive antennas (Ref. 13), and switched wideband (25.25 to 31 GHz) gallium nitride (GaN) HPAs for user terminals as presented in a conference publication and in the expanded version of the same (References 14 and 15). The switched wideband HPA consisted of two separate multistage single-ended HPA chains, each comprising a driver amplifier module and a PA module

interconnected. In the switched wideband HPA, the two single-ended HPA chains operated across the 25.25 to 28 GHz and 28 to 31 GHz frequency bands, respectively. The switching between the two chains is dynamically performed based on the operating frequency band requirements for the terminal at any given moment.

In this report, we extended the above investigations to the design and demonstration of a Ka-band GaN HEMT based MMIC balanced HPA for cognitive radio platforms. The advantages of a balanced HPA (Ref. 16) over a multistage single-ended HPA chain are, first, better stability across the coupler bandwidth because of the good isolation between the two amplification paths or PAs. Second, it provides excellent input and output return loss characteristics because any reflected power is absorbed by the matched loads connected to the isolated ports. This feature provides a constant load impedance to the driver amplifier, which improves gain flatness and phase stability. Third, the HPA gain can be controlled by changing the drain and gate bias voltages without impacting the input/output impedance match or return loss. Fourth, since the input drive power is divided between two PAs, a given amount of gain compression and intermodulation distortion is reached at a 3-dB higher signal drive level than a single-ended amplifier with identical PAs. Fifth, if one of the PAs were to fail, the HPA output power would drop by 6 dB, thus avoiding a catastrophic failure and providing graceful degradation reliability. The disadvantages include greater number of components and consequently higher cost. The results presented here include the balanced HPA output power, gain, PAE, RMS EVM, spectral efficiency, 3rd-order IMD products, spectrum, spectral regrowth, NF, phase noise, and group delay.

2.0 Benefits of Balanced HPA Performance Characteristics Toward Design and Implementation of Cognitive Radio Platforms

The high output power, gain, and wide bandwidth of the HPAs can be exploited by cognitive radios to enable tunability and seamless interoperability across legacy space networks that operate over different frequency bands within the Ka-band spectrum. The high linearity of the HPAs, as demonstrated by the low RMS EVM, enables amplifying higher-order modulation waveforms, such as 8PSK, 16APSK, and 32APSK. This feature also enables cognitive radios to support CCSDS compliant waveforms used in many NASA missions, as well as DVB-S2 waveforms typically used by commercial service providers. The low 3rd-order IMD products generated by the HPAs ensure less spectral regrowth and hence lower interference with adjacent channels. This feature ensures compliance of cognitive radios with the NTIA regulatory standards. Finally, the high PAE of the HPAs reduces power dissipation and improves thermal reliability, thereby enabling small size, weight, and power (SWaP) cognitive radio platforms.

2.1 Use Cases

Lastly, section 6.0 discusses three potential use cases that apply AI and ML techniques and exploit the performance characteristics discussed above such as, tunability, linearity, and low distortion to provide a knowledge-based cognitive radio platform design that improves flexibility, link quality, and interoperability.

3.0 Ka-Band GaN HEMT MMIC Based Balanced HPA Architecture and Brief Set of Specifications Relevant to Cognitive Radio Platform Use Cases

3.1 Balanced HPA Architecture

The architecture of the Ka-band GaN HEMT MMIC based balanced HPA is illustrated in Figure 1. In this architecture, the output waveform from a modulator/up converter is amplified by the balanced HPA and coupled to an antenna for transmission. At the amplifier input, a waveguide-based 3-dB, 90°, hybrid coupler serves as a power divider and splits the output signal from the modulator/up converter (P_{in}) into two paths. In each path, the signal is amplified by a GaN MMIC PA. Next, the outputs from the two PAs are combined using an identical waveguide-based hybrid coupler, which now serves as a power combiner. The combined signal (P_{out}) is routed to an antenna for transmission.

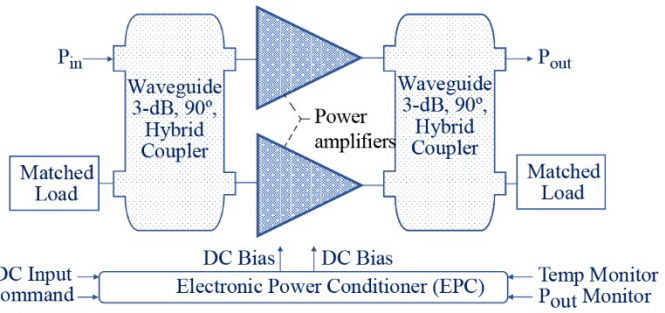

Figure 1.—A simplified GaN HEMT MMIC based Ka-band balanced HPA design architecture. The power amplifiers are Qorvo TGA2595-CP and the waveguide-based (WR-28) 3-dB, 90°, hybrid couplers are manufactured by SAGE (now Eravant). The coupler insertion loss and isolation are on the order of 0.5 and 20 dB, respectively.

An electronic power conditioner (EPC) provides the gate and drain voltages and currents for the power amplifiers. The EPC is a DC-to-DC power convertor that transforms the spacecraft bus voltage, typically in the range of 21 to 35 V, into regulated voltages required by the PAs. In addition, a DC power management circuit is included to manage the correct power-up and power-down sequence. That is to ensure that the negative gate voltages are applied before the positive drain voltages are applied to turn the MMIC amplifiers ON. Furthermore, a DC blanking control is also provided to quickly turn the MMIC amplifiers OFF if a fault condition arises. Moreover, an RF output monitor such as a temperature sensor or a detector/ reference diode pair is located near the PA to monitor for an over temperature condition. The detector/reference diode pair also monitors the RF output power level. The packaged balanced HPA is conduction cooled via its base plate.

3.2 Brief Set of Specifications

- Saturated output power (P_{sat}): 10 to 15 W (CW)
- Bandwidth: 25.25 to 31.0 GHz
- PAE: 18 to 22 percent
- Small signal gain: 28 to 32 dB
- Input/output return loss: < –10.0 dB
- Gain flatness over full bandwidth: <± 1 dB

4.0 RF Performance Validation of the Balanced HPA Design Architecture

To demonstrate the balanced HPA RF performance, the two PA modules and the two waveguide hybrid couplers are assembled into a prototype demonstration model, which is shown in Figure 2. The PAs in the prototype model are capable of operating over a wide frequency range; however, the bandwidth of the available WR-28 waveguide-based hybrid couplers is much narrower and is on the order of 27.5±1.0 GHz. Hence, the measured results reported below are limited to the above frequency range. In the future, to overcome the above bandwidth limitation, we plan to procure WR-34 waveguide-based hybrid couplers that can provide the full 25.25 to 31 GHz bandwidth. Additionally, in our laboratory bench top demonstrations, power supplies from Keysight are employed, instead of an EPC, to provide the required DC voltages and currents to the PAs. Furthermore, the PAs are provided with an integral copper heat sink with forced air cooling to ensure stable and reliable operation.

The performance of the balanced HPA is characterized using a Rohde & Schwarz (R&S) SMW200A Vector Signal Generator, a R&S FSW Signal and Spectrum Analyzer, and a Micronetics Noise Source.

4.1 Output Power, Gain, and Power Added Efficiency

The measured output power (P_{out}) and gain at a carrier frequency or center frequency (f_0) of 27.5 GHz are presented in Figure 3. The operating drain voltages (V_d) and gate voltages (V_g) are indicated in the figure caption. The corresponding PAE is presented in Figure 4. At f_0, the P_{sat} is 41.2 dBm (13.2 W), small signal gain is 30.4 dB, and the peak PAE is 19.3 percent. Similar sets of results have been obtained at the lower and upper band edges frequencies of 26.5 and 28.5 GHz, respectively. The above results are within the specifications indicated previously.

The measured P_{sat} and peak PAE across the 26.5 to 28.5 GHz frequency range is presented in Figure 5 and Figure 6, respectively. The measured gain at saturation and gain at peak PAE across the above frequency range are presented in Figure 7. Figure 7 indicates that the measured gain at peak PAE is on the order of 23.5±1.1 dB.

The small signal gain across the above frequency range is presented in Figure 8. Figure 8 indicates that the small signal gain and the peak-to-peak small signal gain ripple are on the order of 30 dB and ±0.75 dB, respectively.

4.2 Error Vector Magnitude (EVM)

In the past, NASA typically employed constant amplitude type waveforms such as Offset-QPSK for space-to-Earth data transmission. The reason was that the power amplifier could operate at its peak PAE when driven close to saturation and thus conserve spacecraft prime power. However, for future applications, NASA is investigating cognitive radio platforms for user terminals that are capable of roaming and have performance flexibility to interoperate with other space networks for data downlinks. For example, commercial service providers Inmarsat and SES O3b support 8PSK and 16APSK waveforms and data rate of 150 Mbps or greater (Ref. 2). Hence, HPAs that have excellent PAE and linearity to amplify spectrally efficient higher-order modulation waveforms are required. To demonstrate this capability, the EVM at the output of the balanced HPA is measured for the Offset-QPSK, 8PSK, 16APSK, and 32APSK waveform constellations that are typically used in satellite communications. The measurements are performed as a function of P_{in} at a fixed rate of 100 Msymbols per second that is typical for most NASA and commercial applications. The measured EVM for all four Waveforms at a carrier or center frequency of 27.5 GHz is presented in Figure 9 and shows the change in EVM as P_{in} gradually increases from small signal to saturation. At the 1-dB compression point, the RMS EVM is small and less than 6 percent for all four waveforms, which demonstrates good linearity performance.

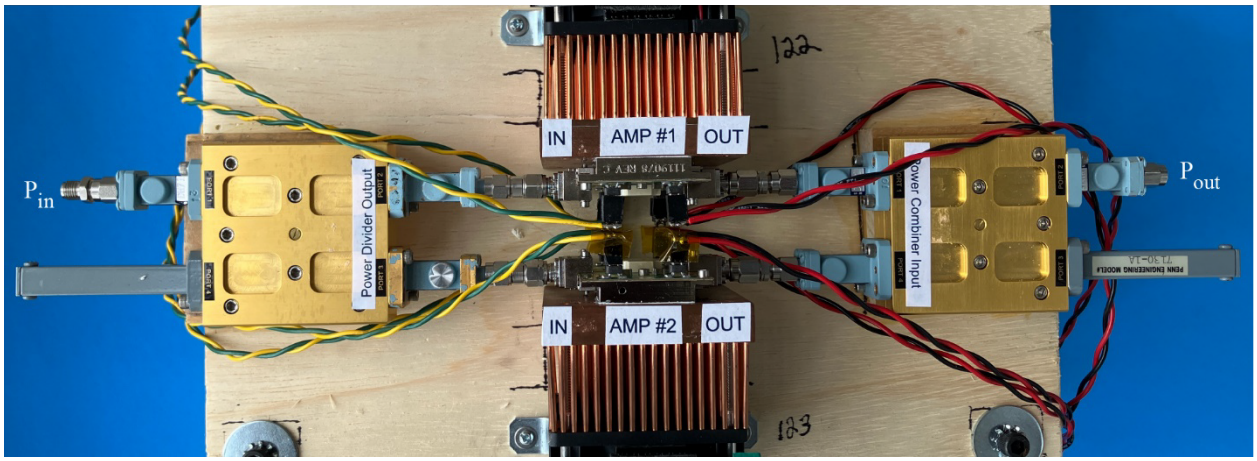

Figure 2.—A prototype demonstration model of a GaN HEMT MMIC based Ka-band balanced HPA.

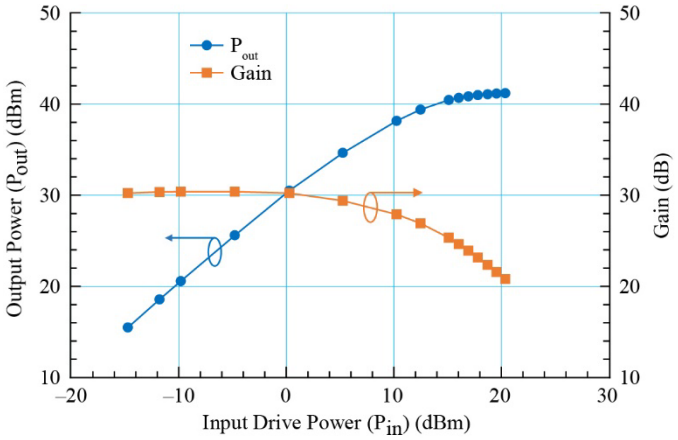

Figure 3.—Measured P_{out} and gain versus P_{in} of the balanced HPA at f_0 = 27.5 GHz. V_{d1} = V_{d2} = 20 V, V_{g1} = –2.2 V, V_{g2} = –2.15 V, T = 25 °C.

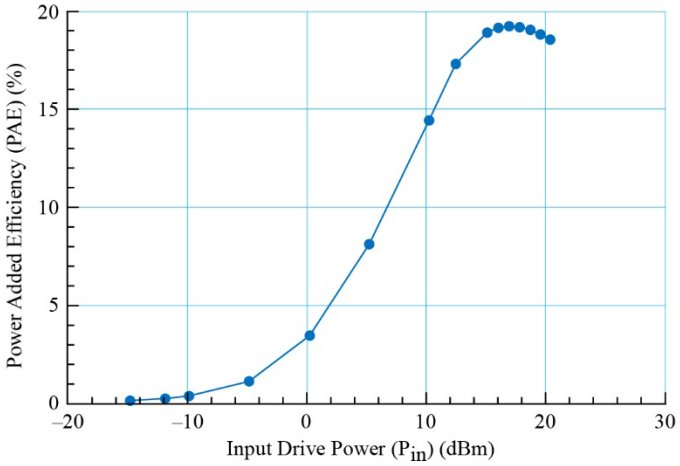

Figure 4.—Measured corresponding PAE versus P_{in} of the balanced HPA at f_0 = 27.5 GHz.

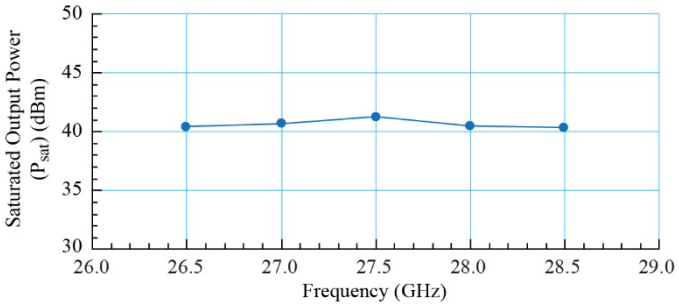

Figure 5.—Measured saturated output power (P_{sat}) versus frequency.

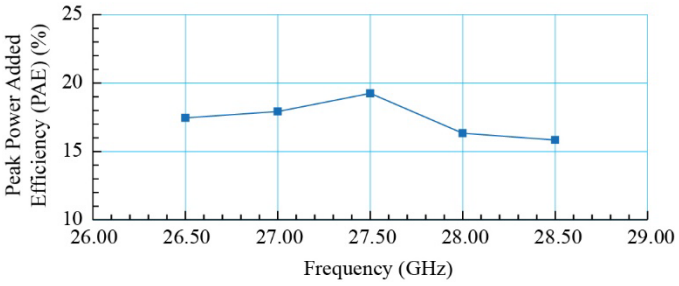

Figure 6.—Measured peak power added efficiency (PAE) versus frequency.

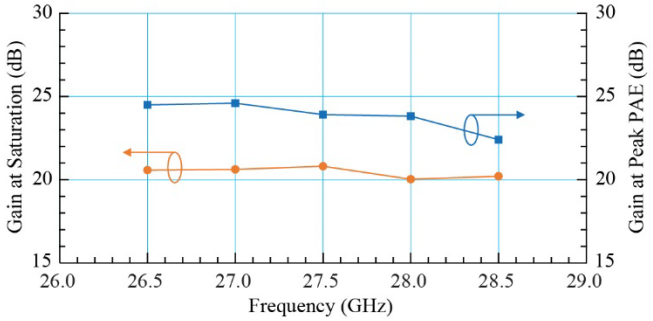

Figure 7.—Measured gain at saturation and gain at peak PAE versus frequency.

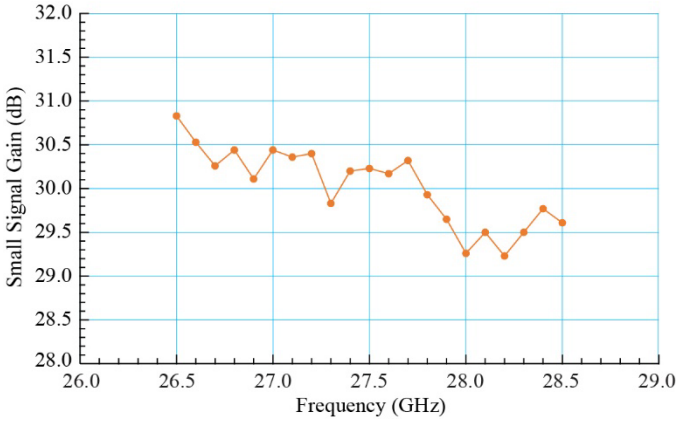

Figure 8.—Measured small signal gain and gain ripple versus frequency. $P_{in} \approx -23.0$ dBm.

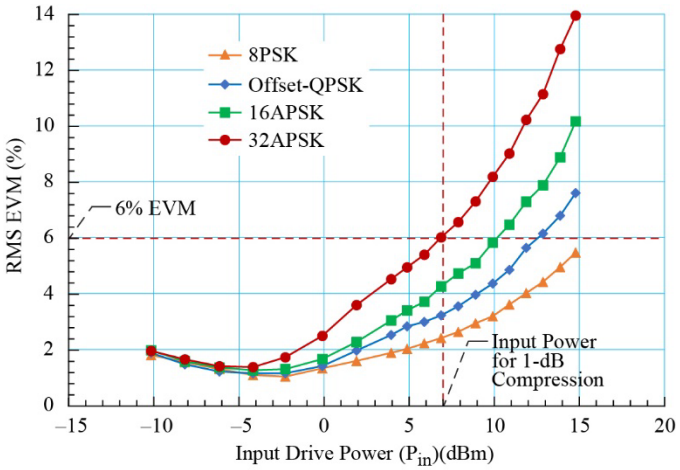

Figure 9.—Measured RMS EVM versus P_{in} at f_0 = 27.5 GHz. The symbol rate is 100 Msymbols per second and the square root raised cosine (SRRC) filter is set to 0.35.

4.3 Spectrum and Spectral Regrowth

The measured spectrum for the four waveforms in Figure 9, when P_{in} is close to the 1-dB compression point, are presented in Figure 10(a) to (d). The results indicate that the spectral efficiency for a fixed bandwidth (135 MHz) increases from 2 bits/s/Hz to 5 bits/s/Hz. Additionally, the spectrum is compliant with the NTIA mask. Furthermore, the out-of-band spectral regrowth measured at 1-symbol rate (100 MHz) away from the carrier or center frequency (f_0 = 27.5 GHz) for all four waveforms is summarized in Table I. The data indicate that the spectral regrowth is less than –30 dBc, which demonstrates low adjacent channel interference or adjacent channel power ratio (ACPR) essential for roaming and interoperability.

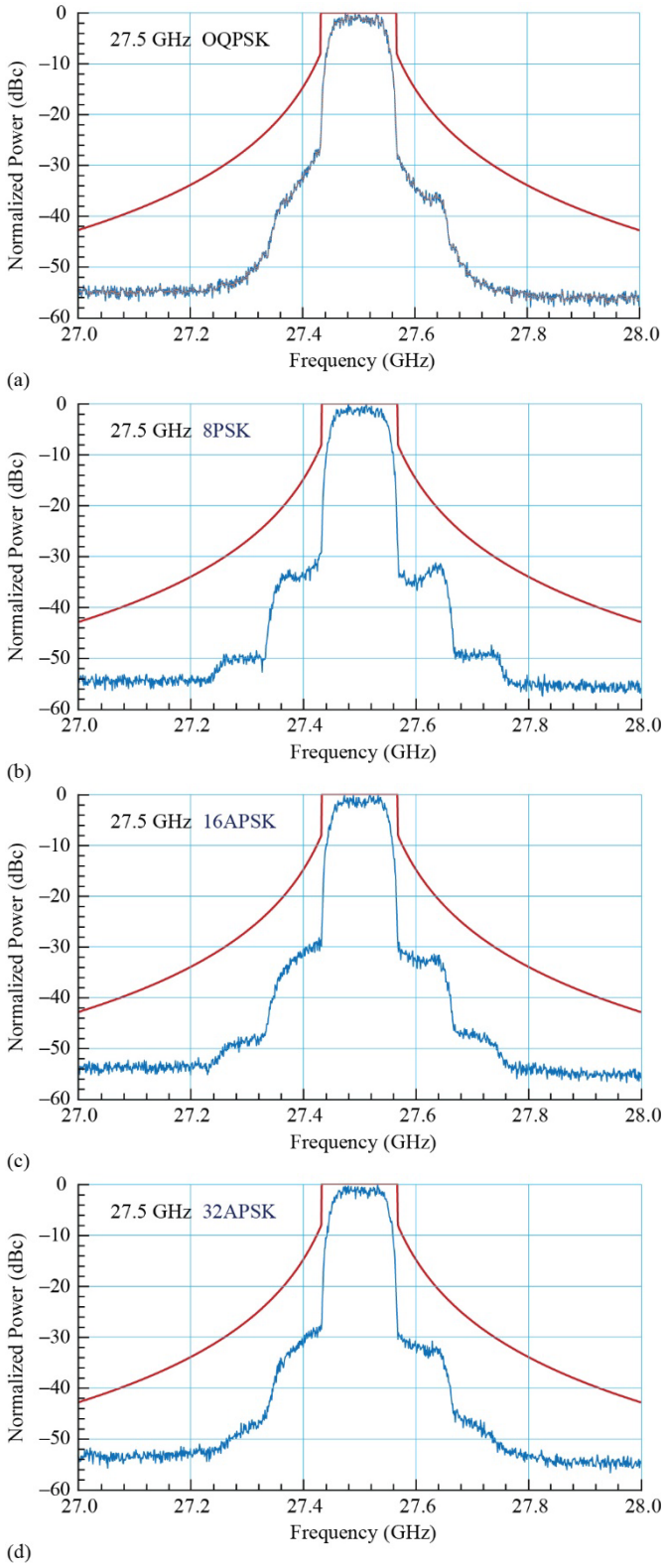

Figure 10.—Measured spectrum. Carrier frequency is 27.5 GHz, symbol rate is 100 Msymbols per second, SRRC filter is set to 0.35, and the bandwidth is 135 MHz. The red solid line is the NTIA emission mask. (a) Offset-QPSK. (b) 8PSK. (c) 16APSK. (d) 32APSK.

TABLE I.—OUT-OF-BAND SPECTRAL REGROWTH

Waveform	Spectral Regrowth (dBc) (@ 27.6 GHz)
Offset-QPSK	–35.1
8PSK	–34.1
16APSk	–32.8
32APSK	–31.5

4.4 3rd-order Intermodulation Products

As discussed earlier, the PAE of the HPA peaks when operated beyond the 1-dB compression point. However, in this mode of operation, the non-linearity of the GaN HEMT generates harmonics and intermodulation distortion signals at the output of the HPA. The harmonic signals are multiples of the fundamental or carrier signal and can be eliminated by using a low-pass filter at the HPA output. However, the intermodulation distortion signals fall within the signal bandwidth and cannot be filtered out and can cause interference. Therefore, the 3rd-order IMD products and the carrier-to-interference ratio (C/I) are measured at a carrier or center frequency of 27.5 GHz and presented in Figure 11 and Figure 12, respectively. The data indicates that the output 3rd-order intercept point (OIP3) is on the order of 56 dBm. The C/I is less than –50.0 dBc initially and gradually increases to about –20.0 dBc as the balanced HPA is driven from small signal to the 1-dB compression and beyond. This feature enables roaming without needing complex lookup tables to prevent adjacent band interference.

4.5 Noise Figure

The measured NF is presented in Figure 13. The NF is less than 9.0 dB across the 26.5 to 28.5 GHz band. A HPA with low NF indicates, that while transmitting, there is less signal-to-noise (S/N) degradation of the adjacent channels. On the other hand, while receiving there is less deviation of the constellation points from their desired locations.

4.6 Phase Noise

Phase noise can cause a rotation of the waveform constellation points. The higher the phase noise, the larger the rotation, which leads to a higher bit error rate (BER). Hence, the phase noise at the output of the HPA is measured. The measured single sideband (SSB) phase noise spectral power density, when P_{out} is close to the 1-dB compression point, is presented in Figure 14. The SSB phase noise spectral power density is in compliance with the envelope defined in the MIL-STD-188-164C and DVB-S2X global interoperability standard.

Similar phase noise characteristics were obtained at the lower and upper band edge frequencies of 26.5 and 28.5 GHz, respectively.

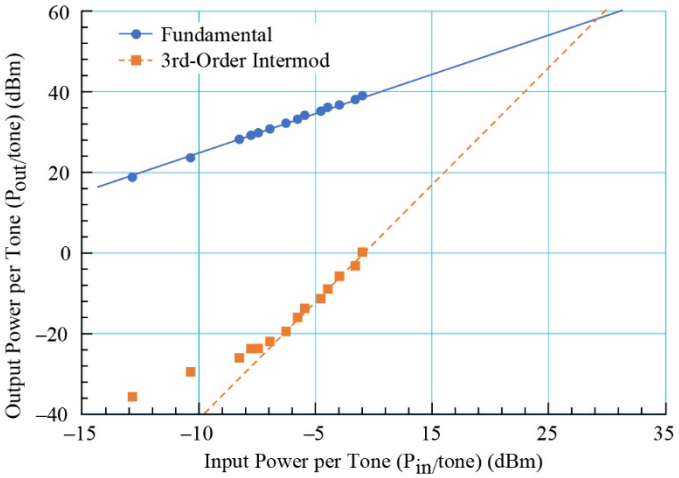

Figure 11.—Measured 3rd-order intermodulation distortion (IMD) versus input power per tone. Tone frequencies are 27.5 GHz ±2.5 MHz. Tone spacing is 5 MHz.

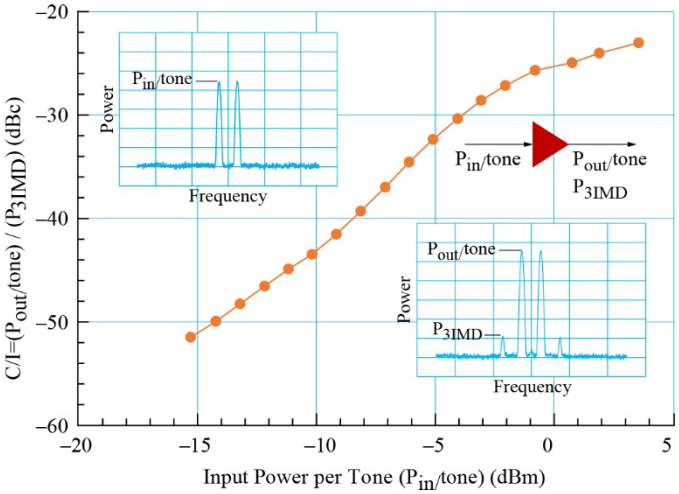

Figure 12.—Measured C/I versus input power per tone. Tone frequencies are 27.5 GHz ±2.5 MHz. Tone spacing is 5 MHz.

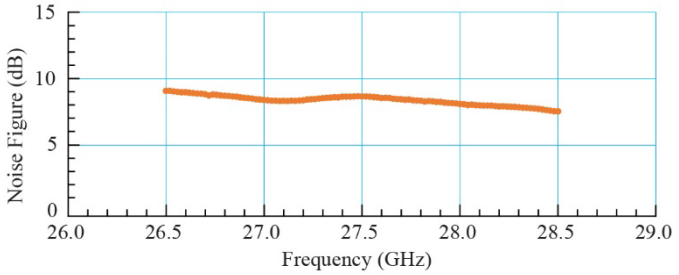

Figure 13.—Measured noise figure versus frequency.

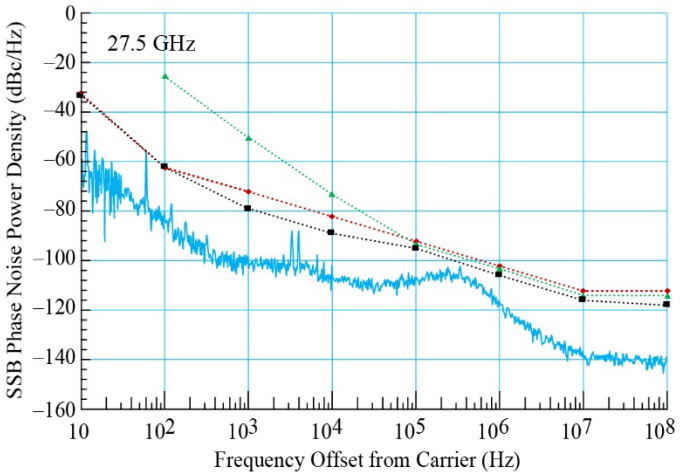

Figure 14.—Measured SSB phase noise spectral power density versus the frequency offset from the carrier frequency. The carrier frequency is 27.5 GHz. The red, green, and black dotted line are the MIL-STD-188-164C, DVB-S2X aggregate phase noise, and professional services masks, respectively.

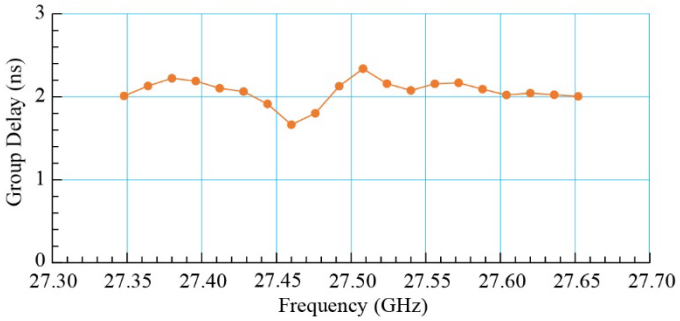

Figure 15.—Measured group delay over a 320 MHz band at a carrier frequency of 27.5 GHz.

4.7 Group Delay

The group delay is a measure of the phase distortion caused by the amplifier and the transit time of the signal through the amplifier. The measured group delay as a function of the frequency is presented in Figure 15. Over a 320 MHz band, centered at 27.5 GHz, the group delay is on the order of 2.0±0.33 ns, which is typical for a balanced amplifier.

5.0 Potential Use Cases for Cognitive Radio Platforms with Wideband Balanced HPA

In this section, as examples, we discuss three potential use cases that apply AI and ML techniques and exploit the balanced HPA performance characteristics discussed earlier to provide a knowledge-based design of cognitive radio platforms for SATCOM.

5.1 Wide Tunable Bandwidth

The ability to tune the operating frequency over a wide frequency range enables interoperability between several space network service providers, especially in the near-Earth domain. This flexibility can be leveraged by an intelligent agent that resides onboard to optimize the selection of a provider by trading several factors, such as cost, latency, and peak data rates, and considering real-time and learned performance, such as weather, availability, and interference (Refs. 2, 3, and 17).

5.2 Performance on Higher-Order Modulation Waveforms

The balanced HPA, because of its excellent linearity, is capable of amplifying higher-order modulation waveforms with low EVM on the order of 6 percent or smaller. This is significant because it allows standards such as DVB-S2 to allow frame-by-frame selection of modulation from QPSK to 32APSK, allowing the onboard intelligent agent to trade reliability versus throughput and spectral efficiency (Refs. 6, 18, and 19).

5.3 Low Intermodulation Distortion Interference

This characteristic is important for a lunar relay satellite that is transmitting data to several user assets on the lunar surface using FDMA techniques. An intelligent agent on the relay satellite could determine which of the several users are within the wide service area on the lunar surface that needs to be contacted at any given time. For instance, in Reference 7, deep reinforced learning is used to perform the allocation of frequencies to users in a relay satellite. It is worth noting that the Space Frequency Coordination Group (SFCG) recommends the use of 23.15 to 23.55 GHz for lunar orbit to lunar surface communications rather than the 25.25 to 31 GHz used in the demonstration above. However, the balanced HPA design architecture presented earlier is flexible and can be scaled to the 23.15 to 23.55 GHz frequency range.

6.0 Conclusions and Discussions

The design architecture and the advantages of a Ka-band GaN HEMT MMIC based balanced HPA are presented. The architecture is validated by characterizing the HPA. The measured output power, gain, PAE, RMS EVM for Offset-QPSK, 8PSK, 16APSK, and 32APSK waveforms, spectral efficiency, 3rd-order IMD products, spectrum, spectral regrowth, NF, phase noise, and group delay are presented and summarized in Table II. The data indicates that the HPA meets

TABLE II.—SUMMARY OF POWER AMPLIFIER TEST RESULTS

Parameter	Measured Value
Frequency range (GHz)	27.5±1.0
Output power (P_{sat}) (dBm)	40.8±0.4 (12.0±1.2 W)
Small signal gain (dB)	30.0±0.75
Peak PAE (%)	17.6±1.7
Gain at peak PAE (dB)	23.5±1.1
Return loss (dB)	< –10.0
RMS EVM for Offset-QPSK, 8PSK, 16APSK, and 32APSK waveforms (%) (P_{in} is at the 1-dB compression point and the carrier frequency is 27.5 GHz)	≤ 6
Out-of-band spectral regrowth (dBc), @ 27.6 GHz	< –30.0
OIP3 (dBm) at a carrier frequency of 27.5 GHz	56
Noise figure (dB) across the frequency range	< 9.0
SSB phase noise power density (dBc/Hz) (Drive at 1-dB compression point)	Compliant with the MIL-STD Mask
Group delay (ns) (At a carrier frequency of 27.5 GHz and over a 320 MHz band)	2.0±0.33

TABLE III.—SUMMARY OF POWER AMPLIFER PERFORMANCE CHARACTERISTICS VERSUS BENEFITS TO COGNITIVE RADIO PLATFORMS

Performance Characteristics	Benefits to Cognitive Radio Platforms
Wide bandwidth	Enables tunability and seamless interoperability across legacy space networks.
High P_{sat}, gain, and PAE	Improves communication distance or range, allows smaller size and mass, and reduces power dissipation, which improves thermal reliability.
Amplifies higher-order waveforms with low EVM	Good linearity, improves spectral efficiency and enhances throughput. Enables supporting CCSDS-compliant waveforms used by NASA and DVB-S2 waveforms used by commercial service providers.
Low out-of-band spectral regrowth	Low adjacent channel interference. Compliance with NTIA mask requirements. Enables roaming and interoperability.
High 3rd-order intercept point (OIP3)	Small interference signals generated within the radio's bandwidth due to amplifier nonlinearity. Enables roaming.
Low noise figure	While transmitting, less S/N degradation of adjacent channels.
Low phase noise	Low rotation of waveform constellation point, which improves BER. Compliance with standards.
Low group delay	Low phase distortion. which improves BER

NTIA, military, and commercial spectral mask requirements and hence enables user terminals that can interoperate and roam. Additionally, the benefits of balanced HPA performance characteristics toward the design and implementation of cognitive radio platforms are presented and summarized in Table III. Lastly, as examples, three potential use cases that exploit AI and ML techniques for cognitive radios with an integrated wideband balanced HPA are discussed. GaN HEMT MMICs enable higher power density and higher PAE, resulting in lighter, smaller, and more efficient HPAs in contrast with prior GaAs based MMIC HPAs.

References

1. NASA Glenn Research Center, Communications Services Project (CSP), https://www1.grc.nasa.gov/space/scan/communications-services-program/
2. M. Piasecki, J. Downey, N. Pham, J. Nessel, A. Gannon, D. Zeleznikar, and M. Koch, "Development and demonstration of a wideband RF user terminal for roaming between Ka-band relay satellite networks," *38th International Communications Satellite Systems Conference (ICSSC 2021) Proceedings*, Arlington, VA, Sept. 27–30, 2021.
3. G.W. Heckler, B.A. Younes, J.W. Mitchell, N.T. Pham, A. Sharma, C. Haskins, and E.L. Weir, "NASA's wideband multilingual terminal efforts as a key building block for a future interoperable communications architecture," *26th Ka Broadband Communications Conference Proceedings*, Arlington, VA, Sept. 27–30, 2021.
4. Special Issue on Artificial Intelligence and Machine Learning Based Technologies for Microwaves, *IEEE Trans Microw Theory Tech,* Part I of two parts, vol. 70, no. 11, Nov. 2022.
5. G. Jo, S. Chan, S. Kim, and D. Oh, "Analysis on the neural network-aided satellite resource allocation schemes," *2023 International Conference on Electronics, Information, and Communication (ICEIC)*, Singapore, Feb. 5-8, 2023.
6. P.V.R. Ferreira, R. Paffenroth, A.M. Wyglinski, T.M. Hackett, S.G. Bilen, R.C. Reinhart, and D.J. Mortensen, "Multiobjective reinforcement learning for cognitive satellite communications using deep neural network ensembles," *IEEE Jour. on Selected Areas in Communications*, vol. 36, no. 5, pp. 1030–1041, May 2018.
7. S. Liu, X. Hu, and W. Wang, "Deep reinforcement learning based dynamic channel allocation algorithm in multibeam satellite systems," *IEEE Access*, vol. 6, pp. 15733–15742, Feb. 26, 2018.

8. Space communications and navigation (SCaN) network projected concept of operations and architecture (PCOA), Section 3, NASA Headquarters, Washington, D.C., Feb. 16, 2023.
9. Y.J.E. Chen, L.Y. Yang, and W.C. Yeh, "An integrated wideband power amplifier for cognitive radio," *IEEE Trans. Microwave Theory Tech*., vol. 55, no. 10, pp. 2053–2058, Oct. 2007.
10. J. Hur, O. Lee, C.H. Lee, K. Lim, J. Laskar, "A multi-level and multi-band Class-D CMOS power amplifier for the LINC system in the cognitive radio application," *IEEE Microwave Wireless Components Lett*., vol. 20, no. 6, pp. 352–354, June 2010.
11. P.C. Huang, Z.M. Tsai, K.Y. Lin, and H. Wang, "A high-efficiency, broadband CMOS power amplifier for cognitive radio applications," *IEEE Trans. Microwave Theory Tech*., vol. 58, no. 12, pp. 3556–3565, Dec. 2010.
12. D. Chelmins, J. Briones, J. Downey, G. Clark, and A. Gannon, "Cognitive communications for NASA space systems," *37th International Communications Satellite Systems Conference (ICSSC 2019) Proceedings*, Okinawa, Japan, Oct. 29–Nov. 1, 2019.
13. R.N. Simons, "Cognitive tapered slot circular array antenna for lunar surface communications," *2021 IEEE Cognitive Communications for Aerospace Applications Workshop (CCAAW)*, Cleveland, OH, June 21–23, 2021.
14. R.N. Simons, J.A. Downey, B.L. Schoenholz, M.T. Piasecki, N.T. Pham, M.K. Siddiqui, and R.G. Bonnin, "Demonstration of a switched wideband GaN high-power amplifier for future space missions," *2023 IEEE Space Hardware and Radio Conference*, Las Vegas, NV, Jan. 22–25, 2023.
15. R.N. Simons, J.A. Downey, B.L. Schoenholz, M.T. Piasecki, N.T. Pham, M.K. Siddiqui, and R.G. Bonnin, "Demonstration of a switched wideband GaN high-power amplifier for future space missions," NASA/Technical Memorandum-20220014361, Dec. 2022.
16. R.S. Engelbrecht and K. Kurokawa, "A wide-band low noise L-band balanced transistor amplifier," *Proc. IEEE*, vol. 53, no. 3, pp. 237–247, March 1965.
17. A. Gannon, S. Paulus, C. Gemelas, and L. Vincent, "Spacecraft-initiated scheduling of commercial communications services," *39th International Communications Satellite Systems Conference (ICSSC 2022) Proceedings*, Stresa, Italy, Oct. 18–21, 2022.
18. J.A. Downey, D.J. Mortensen, M.A. Evans, J.C. Briones, and N. Tollis, "Adaptive coding and modulation experiment with NASA's space communication and navigation testbed," *34th International Communications Satellite Systems Conference (ICSSC 2016) Proceedings*, Cleveland, Ohio, Oct. 18–20, 2016.
19. M.V. Koch and J.A. Downey, "Interference mitigation using cyclic autocorrelation and multi-objective optimization," *NASA Technical Memorandum*, NASA/TM—2019–220226, July 2019.